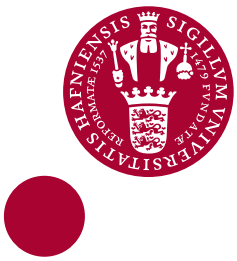

Effects of common groundwater ions on the transformation and reactivity of sulfidized nanoscale zerovalent iron

Mangayayam, Marco C.; Alonso-de-linaje, Virginia; Dideriksen, Knud; Tobler, Dominique J.

Published in:
Chemosphere

DOI:
10.1016/j.chemosphere.2020.126137

Publication date:
2020

Document version
Publisher's PDF, also known as Version of record

Chemosphere 249 (2020) 126137

Contents lists available at ScienceDirect

Chemosphere

journal homepage: www.elsevier.com/locate/chemosphere

Effects of common groundwater ions on the transformation and reactivity of sulfidized nanoscale zerovalent iron

Marco C. Mangayayam [a, *], Virginia Alonso-de-Linaje [b, c], Knud Dideriksen [d], Dominique J. Tobler [a, **]

[a] Nano-Science Center, Department of Chemistry, University of Copenhagen, Universitetsparken 5, 2100, Copenhagen, Denmark
[b] AECOM Environment, Madrid, Spain
[c] GIR-QUESCAT, Departamento de Quimica Inorgánica, Universidad de Salamanca, Salamanca, Spain
[d] Geological Survey of Denmark & Greenland (GEUS), Øster Voldgade 10, 1350, Copenhagen, Denmark

HIGHLIGHTS

- S-nZVI was aged for 7 days in single salt solutions and in real groundwaters.
- S-nZVI corrosion products depended on the dominant ion(s) in the solution.
- Ion concentrations, Fe^0 content, corrosion product, and pH influenced TCE reactivity.

GRAPHICAL ABSTRACT

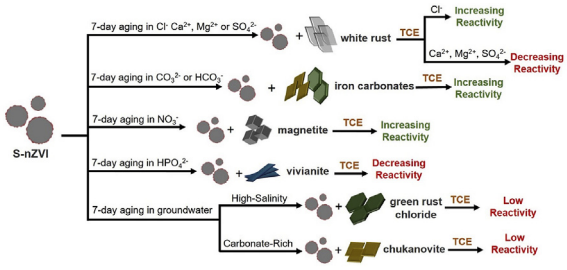

ARTICLE INFO

Article history:
Received 3 October 2019
Received in revised form
29 January 2020
Accepted 5 February 2020
Available online 6 February 2020

Handling Editor: Tsair-Fuh

Keywords:
Corrosion
Metallic iron
Remediation
Trichloroethene
Sulfide
Aging

ABSTRACT

Sulfidized nanoscale zerovalent iron (S-nZVI) is an Fe-based reactant widely studied for its potential use for groundwater remediation. S-nZVI reactivity has been widely investigated testing various contaminants in various water matrices, but studies on S-nZVI corrosion behaviour and reactivity upon exposure to complex groundwater chemistries are limited. Here, we show that anoxic aging of S-nZVI for 7 days in the absence and presence of key groundwater solutes (i.e., Cl^-, SO_4^{2-}, Mg^{2+}, Ca^{2+}, HCO_3^-, CO_3^{2-}, NO_3^-, or HPO_4^{2-}) impacts Fe^0 corrosion extent, corrosion product and reduction rates with trichloroethene (TCE). White rust was the dominant corrosion product in ultrapure water and in SO_4^{2-}, Cl^-, Mg^{2+} or Ca^{2+} solutions; green rust and/or chukanovite formed in HCO_3^- and CO_3^{2-} solutions; magnetite, formed in NO_3^- solutions and vivianite in HPO_4^{2-} solutions. The aged S-nZVI materials expectedly showed lower reactivities with TCE compared to unaged S-nZVI, with reaction rates mainly controlled by ion concentration, Fe^0 corrosion extent, type(s) of corrosion product, and solution pH. Comparison of these results to observations in two types of groundwaters, one from a carbonate-rich aquifer and one from a marine intruded aquifer, showed that S-nZVI corrosion products are likely controlled by the dominant GW solutes, while reactivity with TCE is generally lower than expected, due to the multitude of ion effects. Overall, these results highlight that S-nZVI corrosion behaviour in GW can be manifold, with varied impact on its reactivity. Thus, testing of S-nZVI stability and reactivity under expected field conditions is key to understand its longevity in remediation applications.

* Corresponding author.
** Corresponding author.
E-mail addresses: mc.marco@chem.ku.dk (M.C. Mangayayam), dominique.tobler@nano.ku.dk (D.J. Tobler).

https://doi.org/10.1016/j.chemosphere.2020.126137

1. Introduction

Sulfidized nanoscale zerovalent iron (S-nZVI), produced by reaction of nanoscale zerovalent iron (nZVI) with a sulfide precursor, consists of a metallic iron (Fe^0) core and a nanocrystalline mackinawite-like (FeS_m) shell (Kim et al., 2011; Rajajayavel and Ghoshal, 2015; Gu et al., 2017). The modification results in at least 10-fold increase in trichloroethene (TCE) reduction rates compared to non-sulfidized nZVI (Fan et al., 2017), because the FeS shell limits quick Fe^0 corrosion by water and trace oxygen, while maintaining a conductive surface favourable for TCE reduction (Kim et al., 2011). As such, S-nZVI is a promising alternative to nZVI for *in situ* TCE remediation (Rajajayavel and Ghoshal, 2015; Fan et al., 2016).

The successfulness of *in situ* particle-based remediation often depends on the longevity of the reactant, which generally is first assessed in controlled laboratory environments that mimic subsurface conditions. For nZVI, multiple studies have determined changes in TCE reactivity as a function of aging time (e.g., Liu and Lowry, 2006, Farrell et al., 2000) and/or varying groundwater chemistries (e.g., Liu et al., 2007, Parbs et al., 2007, Chen et al., 2001, Reinsch et al., 2010, Liu et al., 2013). Similar investigations with S-nZVI are, however limited, in particular for S-nZVI produced via two-step synthesis. Fan et al., 2016 and Xu et al., 2019 showed that aging of S-nZVI in oxygen-free deionized water (i.e., absence of solutes) led to a decrease in TCE reduction rate but the aged S-nZVI remained reactive in comparison to unreactive, aged nZVI. Rajajayavel and Ghoshal (2015) showed that the presence of groundwater solutes can significantly lower the reactivity of freshly synthesized S-nZVI. However, little insight was provided as to what caused the reactivity loss. In our recent study, we showed that S-nZVI aged in anoxic artificial groundwater for up to 120 days lost about 50% of its Fe^0 core as a result of anoxic corrosion at FeS_m shell defects after ~10 days. This resulted in the formation of crystalline corrosion products and a ~45% decrease in TCE reduction rates (Mangayayam et al., 2019a). In that study, S-nZVI were aged in a specific artificial groundwater matrix and under static conditions. However, S-nZVI corrosion may proceed faster under more dynamic conditions. Moreover, corrosion behaviour may be different in other groundwater matrices, for example when certain groundwater solute(s) dominate (i.e., Na^+ and Cl^- in seawater intruded aquifers, or Ca^{2+}, Mg^{2+}, and HCO_3^- in limestone aquifers). To the best of our knowledge, there are no systematic investigations on the effects of common groundwater solutes on S-nZVI structure and reactivity. This understanding may be needed to help predict S-nZVI longevity during *in situ* subsurface remediation.

In this study, we assessed changes in S-nZVI structure and TCE reduction rate after 7-day exposure to solutions of common groundwater ions to identify the solutes that could impact most on S-nZVI longevity in groundwaters. Specifically, we tested the effects of $MgCl_2$, $CaCl_2$, $NaCl_2$, Na_2SO_4, $NaHCO_3$, Na_2CO_3, $NaNO_3$, and Na_2HPO_4, at concentrations typical for groundwater, on S-nZVI aging. In addition, identical experiments were performed using two different groundwaters, one from a marine intruded aquifer in Spain and one from a carbonate-rich aquifer in Denmark, to assess if observations from simple, single salt systems can be used to predict S-nZVI behaviour in complex groundwaters. S-nZVI structural changes were determined using synchrotron-based X-ray scattering techniques and scanning electron microscopy, while gas-chromatography mass spectrometry was used to determine rates of TCE degradation.

2. Materials and methods

Unless stated otherwise, all syntheses and preparations for aging, reactivity experiments and sample characterization were performed inside an anoxic vinyl-walled glovebox (95% N_2/5%H_2; Coy laboratories) using reagent grade chemicals and deoxygenated, ultrapure water (MilliQ, resistivity $\geq$ 18 MΩcm, sparged with N_2 for 24 h). Air intrusion and TCE outgassing during aging and reactivity experiments were minimized by the use of Viton™ rubber stoppers and crimp seals, a low-headspace to solution ratio and by placing the reactors horizontally to avoid contact between Viton™ rubber stopper and headspace (Mangayayam et al., 2018). Information on reagents can be found in supplementary information, SI, Text S1. Two types of groundwaters (GW) were collected from wells: one from a carbonate rich aquifer (GW_{HARD}) in Skovlunde, Denmark and one from a marine intruded aquifer (GW_{SALINE}) in Baix Llobregat, Catalunya, Spain (SI, Text S2, Table S1).

2.1. S-nZVI synthesis

S-nZVI was synthesized following a modified two-step synthesis by Rajajayavel and Ghoshal, 2015, identical to our previous study (Mangayayam et al., 2019a). Briefly, 35.8 mL of 1.1 M sodium borohydride (BH_4^-) solution were titrated (5 mL/min) to 71.6 mL of 0.25 M $FeCl_2$ in 30% ethanol (in MilliQ water). The suspension was stirred for another 10 min before separating the particles using a strong magnet. The particles were re-suspended in 120.8 mL of 0.2 M acetate buffer solution in a 160 mL serum bottle, crimp capped and sonicated for 15 min outside the glovebox. Then, 4.2 mL of 1 M Na_2S solution were injected through the Viton™ stopper to initiate sulfidation, and the bottle was sonicated for another 10 min, before placing it on an orbital shaker (200 rpm) for 3 h. After sulfidation, the solids were washed with N_2 sparged O_2-free ethanol using a 3-fold rinse cycle and separated by vacuum filtration (inside anoxic glovebox). The washed S-nZVIs were resuspended in 100 mL MilliQ water (theoretical mass loading = 10 g L^{-1} and S/Fe synthesis ratio = 0.23) and immediately used for aging and reactivity experiments.

2.2. S-nZVI aging and TCE reactivity

S-nZVI was aged in the absence (i.e., degassed MilliQ water only) and presence of common groundwater solutes (SI, Table S2) under constant shaking at room temperature. The impact of varying anion concentrations (Cl^-, SO_4^{2-}, HCO_3^-, CO_3^{2-}, NO_3^-, HPO_4^{2-}) were tested using their sodium (Na^+) salts, assuming that Na^+ has negligible impact on reactions (Liu et al., 2007; Devlin and Allin, 2005). For divalent cations (Mg^{2+} and Ca^{2+}), chloride (Cl^-) salts were used. The ion concentration ranges were chosen according to their variability in real groundwater systems (e.g., Table S1). Additionally, S-nZVI was aged in the collected groundwaters to assess the combined effects of multiple groundwater solutes on particle aging and reactivity (SI, Table S1).

For the aging experiments, aliquots of the S-nZVI suspensions in MilliQ water were added to the prepared salt solutions or to the collected GW inside 60 mL serum bottles to have a final volume of 50 mL and solid concentration of 0.5 g L^{-1}. The varying salt concentrations are specified in Table S2. Each condition was tested in triplicate. The solutions were left unbuffered to minimize influences of other ions. This resulted in initial pH being neutral except for HCO_3^- (pH = 8.1–8.2), CO_3^{2-} (pH = 10.5–10.8), and the collected groundwaters (pH = 7.6 ± 0.1 and 7.8 ± 0.1). The reactors were crimp capped and left to age on an orbital shaker (150 rpm) for 7 days to accelerate particle-ion interaction. The solution pH was measured after aging (SI, Table S2).

After 7-day aging, two of the triplicate reactors were amended with 25 μL of 10,000 ppm (v/v) TCE (in methanol) to yield 55 μM TCE, and then re-capped and shaken as before (inside the

glovebox). TCE controls in the tested water matrices (i.e., the different salt solutions and the two groundwater matrices with no added S-nZVI) were set up in parallel and used to normalize the TCE loss over time. Regular suspension sampling for TCE analyses by gas chromatography − mass spectroscopy was performed over 50 h as previously described (SI, Text S3) (Mangayayam et al., 2018). The third reactor was sacrificed to characterize the aged S-nZVI material. For this, all solids in the reactors were separated from the supernatant using a magnet (i.e., supernatant free from precipitates based on visual inspection), rinsed once with ~50 mL degassed MilliQ, vacuum filtered (0.2 μm) and then dried in a desiccator under vacuum (48 h at 22 °C).

2.3. S-nZVI characterization

High energy X-ray scattering measurements were performed at beamline 11-ID-B (58 keV, $\lambda = 0.2114$ Å), Advanced Photon Source (APS), Argonne National Laboratory (USA) to probe structural changes resulting from S-nZVI aging. Scattered X-rays were detected by a 40 × 40 cm amorphous Si 2D detector (PerkinElmer) at a sample-to-detector distance of 1000 mm for high energy X-ray diffraction (HEXRD), and 180 mm for pair distribution function (PDF) analysis. Prior to transport to APS, dried samples were filled into glass capillaries and sealed with paraffin, ensuring that samples were under anoxic atmosphere during transport and measurements (Dideriksen et al., 2015). An empty glass capillary and a CeO_2 standard were measured for background correction and for sample-detector geometry calibration. Fit-2D (Farrow et al., 2007) was used for calibration and integration of the data to 1D scattering patterns. OriginPro was used to fit Gaussian curves to low R (0.5−3.5 Å) PDF peaks to approximate the residual Fe^0 content (atomic %) in the aged products, as performed in our previous study (Mangayayam et al., 2019a). Details of the fitting procedure are described in SI, Text S4, Fig. S1. For scanning electron microscopy (SEM), suspensions were diluted by a factor of 10 in MilliQ water and then directly pipetted onto an aluminium stub and left to dry for 30 min in a desiccator under vacuum (inside anoxic glovebox). The samples were imaged using a FEI Quanta 3D FEG SEM at 7 kV and 8.7 pA with a secondary electron detector. Electron dispersive X-ray spectroscopy maps were acquired using a FEI tecnai G20 F20 X-Twin FEG S/TEM operated at 200 kV, a Fischione high angle annular dark field detector and an EDAX X-ray analyzer.

3. Results and discussion

3.1. Characterization of unaged S-nZVI

HEXRD of unaged S-nZVI shows peaks corresponding to metallic iron ((110) Fe^0 at 3.1 $Å^{-1}$) and a mackinawite-like phase ((001) FeS_m at 1.19 $Å^{-1}$, SI, Fig. S2). SEM images of this material show the typical chain-like aggregates expected for ferromagnetic nanoparticles, with S-nZVI particles sizes around 50−150 nm in diameter (SI, Fig. S3). EDXS maps reveal that S-nZVI have a sulfur to iron ratio of ~0.04 (SI, Fig. S4). These structural, morphological and compositional features match well with the HEXRD and HRTEM images in our previous study (Mangayayam et al., 2019a), suggesting that the S-nZVI synthesized here has as an Fe^0 core and FeS_m shell. In terms of TCE reduction rate, the fitted pseudo-first order rate constant (k_i) for unaged S-nZVI was 0.173 ± 0.003 h^{-1} (SI, Table S2).

3.2. Structure and reactivity of 7 days aged S-nZVI

3.2.1. Aging in MilliQ water (reference experiment)

S-nZVI was aged in MilliQ water to provide a baseline for determining the effects of common groundwater ions. HEXRD shows peaks for Fe^0 and FeS_m stemming from S-nZVI and additional peaks characteristic for ferrous hydroxide ($Fe(OH)_2$), often called white rust (labelled WR in Fig. 1a and b). This was confirmed by SEM images showing chain-like S-nZVI aggregates surrounded by thin, hexagonal flakes characteristic of white rust (Fig. S5). Based on PDF peak intensities, about 22% of the initial Fe^0 cores were oxidized to white rust after 7-day aging (Table S2). The solution pH increased from neutral to 9.1 ± 0.1, as would be expected from OH^- production during water reduction (Equation (1)) (Furukawa et al., 2002). We argue that crystal defects in the FeS_m shell enabled anoxic corrosion as proposed previously (Mangayayam et al., 2019a), while the basic pH conditions led to white rust precipitation (Equation (2)). Aging occurred faster in these experiments compared to our previous static aging experiments (Mangayayam et al., 2019a), most likely because the reactors were shaken throughout aging.

$$Fe^0 + 2H_2O \rightarrow Fe^{2+} + 2OH^- + H_2 \quad (1)$$

$$Fe^{2+} + 2OH^- \rightarrow Fe(OH)_2 \quad (2)$$

In terms of TCE reactivity, the MilliQ aged S-nZVI exhibited a lower reduction rate ($k_{aged} = 0.10\ h^{-1}$) compared to the unaged S-nZVI ($k_i = 0.17\ h^{-1}$, SI, Table S2, Fig. S6). This decrease in reactivity can be partly explained by the substantial loss in Fe^0 core material (~22%), in comparison to unaged S-nZVI (Mangayayam et al., 2019a). Another factor that likely contributed to the reactivity decrease is the formation of white rust. White rust is dominantly protonated (i.e., $\equiv Fe{-}OH_2^+$) at the pH (9.1) monitored here (point of zero charge, pH_{PZC}, of white rust = 12.1 ± 0.1) (Yoon et al., 1979; Schott, 1977; Parks, 1965), while S-nZVI surface sites (i.e., $\equiv Fe{-}S^-$) are dominantly deprotonated (pH_{PZC} of FeS = 7.5 ± 0.1) (Wolthers et al., 2005). As such, attractive electrostatic interactions may have led to a close association between white rust and S-nZVI particles, also indicated by SEM images (Fig. S5). In turn, this could have lowered accessibility for TCE to FeS_m surface sites (argued to be the active sites for TCE reduction) (Butler and Hayes, 1998, 2001), and hence lowered TCE reduction rates (Kim et al., 2011; Rajajayavel and Ghoshal, 2015; Chen et al., 2001; Butler and Hayes, 2001).

3.2.2. Influence of Cl^- and SO_4^{2-}

Similar to S-nZVI aged in MilliQ water, white rust is the main corrosion product when S-nZVI was aged in chloride (Cl^-) or sulfate (SO_4^{2-}) solutions as shown by HEXRD (Fig. 1a and b) and SEM (Fig. 1c and d). Interestingly, S-nZVI aged in Cl^- solutions exhibit substantially less Fe^0 corrosion (SI, Table S2), i.e., less white rust formation, compared to S-nZVI aged in MilliQ, while S-nZVI aging in SO_4^{2-} solutions led to enhanced Fe^0 corrosion. These trends are also evidenced by the relative white rust HEXRD peak intensities (Fig. 1a and b) and relative white rust abundances in SEM images (Fig. 1c and d). Notably, the extent of Fe^0 corrosion was marginally affected by the increase in Cl^- or SO_4^{2-} concentration, respectively.

An exception to above observations is the S-nZVI material aged in 700 mM Cl^- solution (mimicking seawater-like conditions), where chloride green rust (Fe^{2+}, Fe^{3+} layered hydroxide with interlayer chloride, G_{RCl}) appeared as the only corrosion product, based on small but noticeable HEXRD peaks and hexagonal, micron-sized platelet in SEM (Fig. S7). Under anoxic conditions, trace Fe^{3+} may be produced from the oxidation of white rust via Schikorr reaction (Reardon, 1995). However, such a process seems unlikely here considering that we do not see any structural evidence of mixed-valent iron phases in the other tested Cl^- and SO_4^{2-} solutions, or MilliQ water. Considering the overall low abundance of this Fe^{3+}-bearing corrosion product, it is therefore more likely that

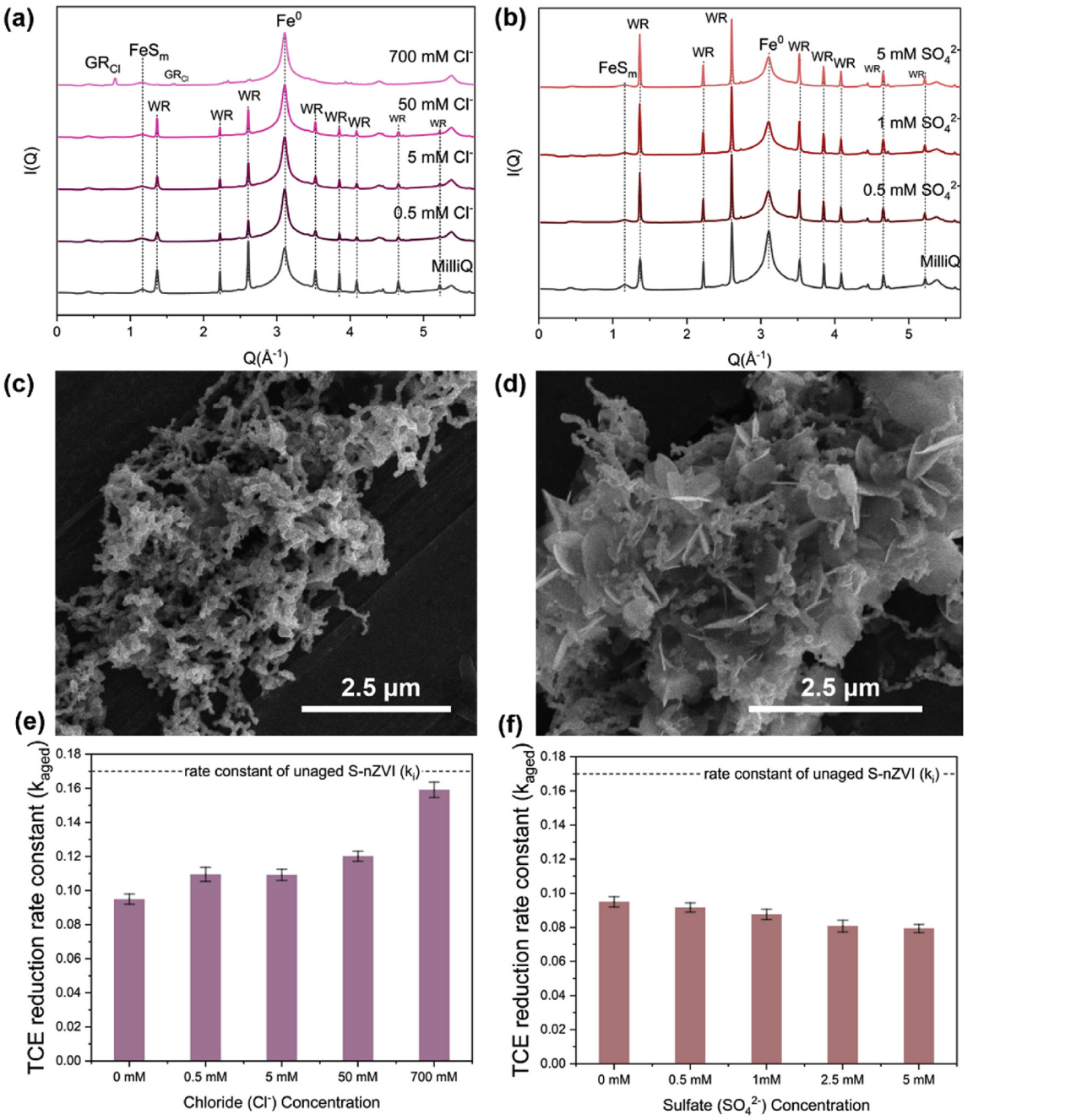

Fig. 1. HEXRD patterns of S-nZVI aged in solutions with increasing (a) Cl^- and (b) SO_4^{2-} concentration (added as Na-salts). For comparison, the HEXRD pattern of the MilliQ-aged S-nZVI (reference experiment) is also shown. Reflections are annotated as Fe^0 and FeS_m for S-nZVI core and shell; WR for white rust; and GR_{Cl} for chloride green rust. SEM images of S-nZVI aged in (c) 5 mM Cl^- and (d) 5 mM SO_4^{2-} solutions, both still showing initial S-nZVI chain aggregates. In addition, the SO_4^{2-} aged S-nZVI exhibit abundant thin, hexagonal shaped flakes characteristic of white rust, which are rare in Cl^- aged S-nZVI. TCE reduction rate constants of S-nZVI aged in solutions with increasing (e) Cl^- and (f) SO_4^{2-} concentrations. For comparison, the TCE reduction rate constant of unaged S-nZVI (k_i) is plotted as a dashed line. (For interpretation of the references to colour in this figure legend, the reader is referred to the Web version of this article.)

it formed during material exposure to trace oxygen during reactor sampling and/or sample drying for characterization. Indeed, fast oxidation rates have been observed for Fe^{2+} in the presence of high Cl^- concentratons (Po and Sutin, 1968).

Exposure of microscale ZVI to SO_4^{2-} and Cl^- solutions is well known to induce corrosion (Devlin and Allin, 2005; Johnson et al., 1697). As such, it was expected that these anions enhance Fe^0 corrosion at FeS_m defects on S-nZVI surfaces. The observed increased Fe^0 corrosion and white rust formation in the presence of SO_4^{2-} supports this assumption (SI, Table S2). In Cl^- solutions, the trend is however different: white rust formation is generally lower and Fe^0 content after aging is higher compared to the MilliQ system. Note that the pH in Cl^- and SO_4^{2-} solutions were comparable after aging with S-nZVI (9.1 ± 0.1, SI, Table S2), indicating that pH would not have influenced the observed difference in Fe^0 corrosion extent between these two anions.

Similar to the MilliQ system, aging of S-nZVI in Cl^- and SO_4^{2-} solutions negatively impacted TCE reduction rates (k_{aged}), compared to unaged S-nZVI (k_i, Fig. 1e and f, Fig. S6). Generally, k_{aged} values were higher in Cl^- solutions than in SO_4^{2-} solutions.

These trends may be best explained by the extent in S-nZVI corrosion, with less Fe^0 corrosion and less white rust formation observed in Cl^- solutions compared to SO_4^{2-} solutions. In addition, differences in reactivity were also observed upon varying Cl^- and SO_4^{2-} concentration: k_{aged} increased with increasing Cl^- concentration, while it decreased with increasing SO_4^{2-} concentration (Fig. 1e and f, Fig. S6). Fe^0 corrosion extent, white rust abundance and pH little fluctuated with increasing anion concentration, suggesting that these parameters had little impact on the changes in TCE k_{aged} with increasing ion concentration. Instead, it is the ions that somehow enhance (i.e., Cl^-) and limit (i.e., SO_4^{2-}) TCE reactivity with increasing concentration.

3.2.3. Influence of Ca^{2+} and Mg^{2+}

Aging of S-nZVI in solutions with variable concentrations of calcium (Ca^{2+}) or magnesium (Mg^{2+}) ions led to similar extents of Fe^0 corrosion, white rust formation (Fig. 2a and b; SI, Table S2) and solution pH (pH = 9.1 ± 0.1) as observed for S-nZVI aged in MilliQ water. These observations suggest that these cations had negligible effect on S-nZVI corrosion behaviour. These observations are somewhat in constrast to previous studies on S-nZVI (produced with one-pot synthesis) (Kim et al., 2013, 2014) and ZVI (Liu et al., 2013, 2014) that argued that both Mg^{2+} and Ca^{2+} (at similar concentrations as used here) induce surface corrosion. Notably, surface characteristics are different between different S-nZVI particles and ZVI (Mangayayam et al., 2019a, 2019b), thus surface processes will likely differ between these systems.

In terms of TCE reactivity by S-nZVI aged in Mg^{2+} and Ca^{2+} solutions, different trends were observed for these cations: k_{aged} increased with increasing Mg^{2+} concentration, while it decreased with increasing Ca^{2+} concentration (Fig. 2c and d, Fig. S6). These systematic changes in TCE reduction rate with cation concentration, while other observed parameters (i.e., extent of Fe^0 corrosion, white rust formation, and pH) remained fairly constant, indicate that TCE reduction is somewhat enhanced in the presence of Mg^{2+} but inhibited by Ca^{2+}. It is unclear what controls these opposite trends in TCE reactivity, particularly seeing that both cations have been shown to adsorb well on FeS_m surfaces (Wolthers et al., 2005; Morse and Arakaki, 1993). Notably, Kim et al. (2013) also observed higher TCE reactivity by S-nZVI (produced with one-pot synthesis) in the presence of Mg^{2+}, while Ca^{2+} stimulating effects were lower. Similarly, Liu et al. (2014) showed that TCE reduction by passivated ZVI (i.e., with iron oxide shell) is enhanced in the presence of Mg^{2+} solutions but not in Ca^{2+} solutions. They explained this by Mg^{2+} inducing dissolution of surface corrosion products, while Ca^{2+} cannot. Dong et al. (Dong and Lo, 2013), on the other hand, showed that Ca^{2+} ions induce aggregation of nZVI particles, that could potentially lead to a decrease in reactive surface sites.

3.2.4. Influence of HCO_3^- and CO_3^{2-}

S-nZVI aged in various bicarbonate (HCO_3^-) and carbonate (CO_3^{2-}) solutions exhibited Fe^0 corrosion extents (Table S2) that were comparable to observations in the MilliQ system. The type of corrosion product differed, however, with carbonate green rust (GR_{CO3}) forming at most HCO_3^-/CO_3^{2-} concentrations, except for solutions containing 10 mM HCO_3^-, where chukanovite was the main corrosion product (Fig. 3a and b). SEM images show hexagonal plates characteristic of GR_{CO3} and thin rhomboidal sheets as previously observed for chukanovite (Fig. 3c and d) (Yang and Akid, 2015; Pekov et al., 2007). These iron-carbonate phases are common

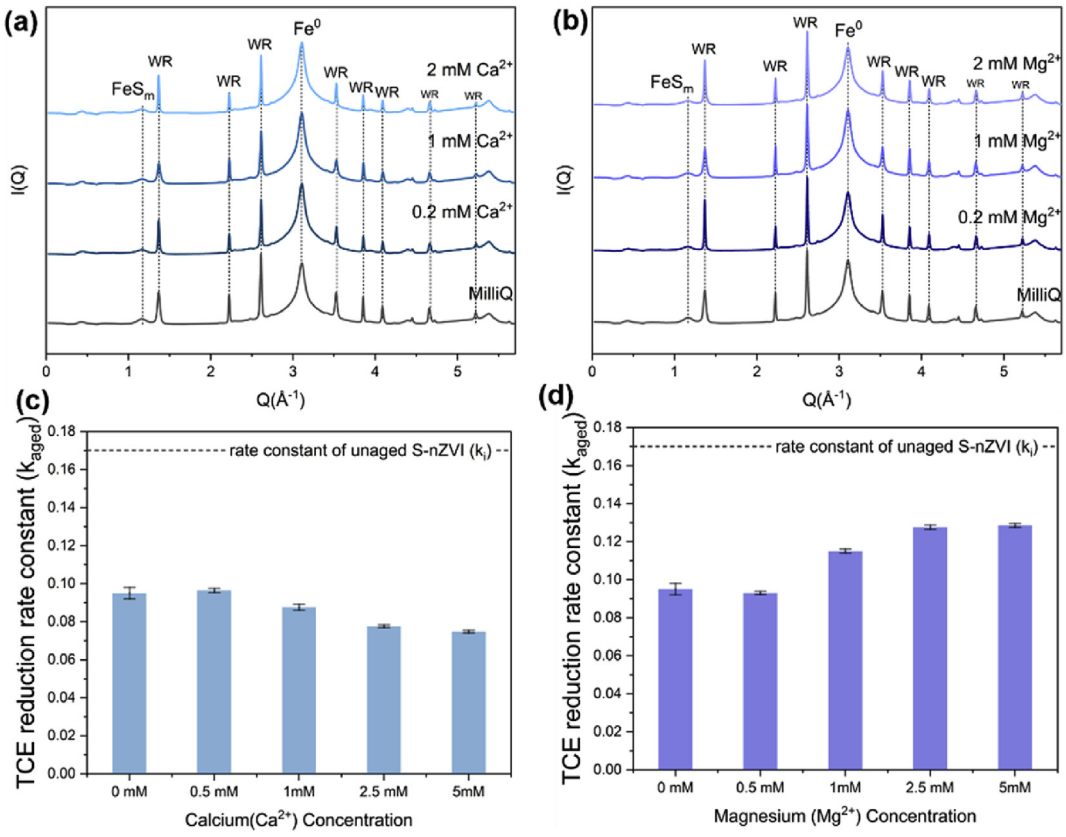

Fig. 2. HEXRD patterns of S-nZVI aged in solutions with increasing (a) Ca^{2+} and (b) Mg^{2+} concentration (added as Cl^- salt). The main corrosion product that formed was white rust (WR). The reflections stemming from S-nZVI core and shell are annotated as Fe^0 and FeS_m. TCE reduction rate constants of S-nZVI aged in solutions with increasing (c) Ca^{2+} and (d) Mg^{2+} concentrations. The rate constant (k_i) obtained for the unaged S-nZVI material is indicated by the dashed line.

Fe^0 corrosion products in carbonate-rich, anoxic waters and at the alkaline pHs monitored here (Chen et al., 2016; Drissi et al., 1995). Note that chukanovite was absent in CO_3^{2-} solutions and this may be explained by the substantially higher pH (pH = 10.9–11.2) in CO_3^{2-} solutions, compared to HCO_3^- solutions (pH = 9.1–9.5, Table S1) (Chen et al., 2016). The presence of substantial amounts of carbonate green rust in almost all HCO_3^-/CO_3^{2-} aging experiments suggests that Fe^{3+} formed via a specific oxidation process enabled by the activity of these anions, rather than accidential oxidation during sampling (as we argued for minor GR_{Cl} formation in experiments with 700 mM Cl^-; section 3.2.2). In a previous study, Fe^{3+} was shown to form during CO_2 reduction at iron sulfide electrodes (Roldan et al., 2015). Whether such a process could have acted here however, is uncertain, but may be worth investigating in future studies.

Compared to unaged S-nZVI, S-nZVI aging in HCO_3^- or CO_3^{2-} solutions also negatively impacted TCE reduction rates. Generally, however, k_{aged} values in the presence of these anions were higher than in the MilliQ system, despite similarities in Fe^0 corrosion extent. Partly, this may be explained by the differences in corrosion products. Here, GR_{CO3} and/or chukanovite formed instead of white rust. These iron-carbonates will be dominantly deprotonated (PZC around 7.9 ± 0.1) (Biegler and Houchin, 1986; Génin et al., 2005), similar to S-nZVI surfaces, at the monitored pHs (Table S2). Thus, iron-carbonates and S-nZVI may interact less with each other (i.e., less aggregation), meaning FeS_m site availability may be higher than in the presence of white rust, which could in parts explain why

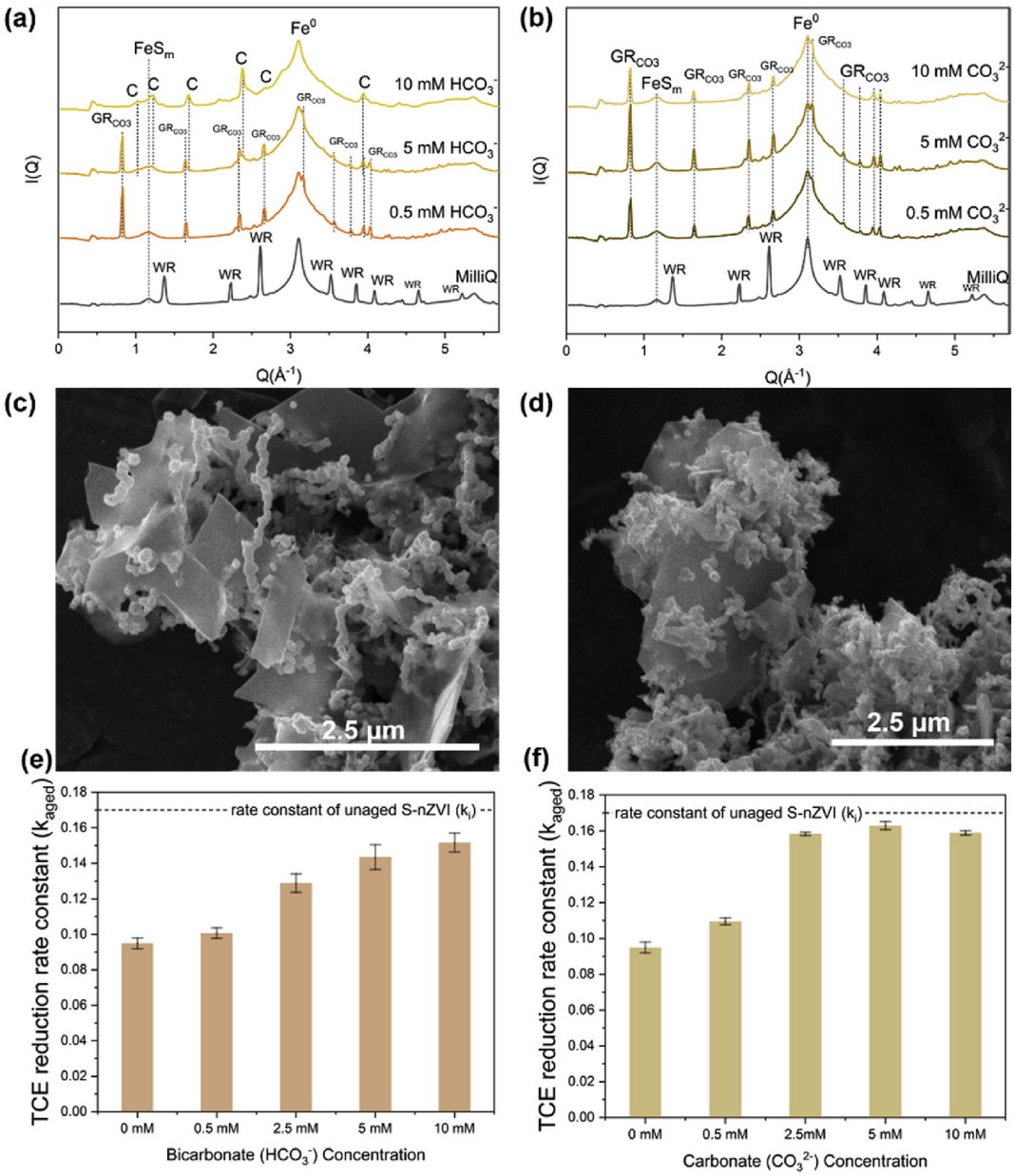

Fig. 3. HEXRD patterns of S-nZVI aged in solutions with increasing (a) HCO_3^- and (b) CO_3^{2-} concentration (added as Na-salts). HEXRD reflections of S-nZVI core and shell are denoted as Fe^0 and FeS_m. The main corrosion products were carbonate green rust (GR_{CO3}) and chukanovite (C). SEM images of S-nZVI aged in (c) 5 mM HCO_3^- solutions and in (c) 5 mM CO_3^{2-} show corrosion products along with S-nZVI particles. TCE reduction rate constants of S-nZVI aged in solutions with increasing (e) HCO_3^- and (f) CO_3^{2-} concentrations. For comparison, the TCE reduction rate of unaged S-nZVI (k_i) is indicated by the dashed line. (For interpretation of the references to colour in this figure legend, the reader is referred to the Web version of this article.)

TCE reactivity in HCO_3^- or CO_3^{2-} solutions is higher compared to the MilliQ system. An additional observation was that k_{aged} increased with increasing HCO_3^- or CO_3^{2-} concentrations (Fig. 3c, d, Fig. S6), indicating that similar to systems discussed above (e.g., Mg^{2+}, Ca^{2+}, Cl^-, and SO_4^{2-}), TCE reduction was somewhat also affected by the presence of these ions.

A last observation concerns the generally higher TCE reactivities in CO_3^{2-} solutions compared to HCO_3^- solutions, despite similarities in Fe^0 content and corrosion product. Likely, this is partly due to the substantially higher pH values in CO_3^{2-} solutions compared to HCO_3^- solutions. For example, Rajajayavel and Ghoshal, 2015 showed 75% increase in TCE reduction rates by S-nZVI upon pH increase from 9.0 to 11.0. The authors argued that higher pH led to higher abundance of reactive, deprotonated ≡Fe−S$^-$ sites on S-nZVI (Wolthers et al., 2005), thereby increasing the sites for TCE degradation (Rajajayavel and Ghoshal, 2015; Kim et al., 2013).

3.3. Influence of NO_3^-

S-nZVI aged in nitrate (NO_3^-) solutions exhibited an increase in Fe^0 corrosion with increasing NO_3^-concentrations (SI, Table S2), which was accompanied by the formation of a spinel phase, presumably magnetite (Fe_3O_4), as shown by HEXRD and SEM (Fig. 4a and b). These observations strongly indicate that NO_3^- was reduced by S-nZVI, utilizing electrons from the Fe^0 core. This is also supported by the systematic pH increase (i.e., H^+ consumption by NO_3^- reduction) observed during aging (SI, Table S2). In nZVI systems, it has been shown that NO_3^- reduction led to quick surface passivation by magnetite or maghemite formation, which then limited further corrosion (Liu et al., 2006, 2007; Reinsch et al., 2010; Su et al., 2012). Here, S-nZVI aged in NO_3^- solutions only exhibited a spinel phase, which seemed to form separate and discrete cubic particles (Fig. 4b).

Despite substantial Fe^0 corrosion during aging (i.e., NO_3^- reduction), k_{aged} values were still comparable to the MilliQ system, and seemed to be higher (about 20%) when S-nZVI was aged under higher NO_3^- concentrations (Fig. 4c, Fig. S6). Considering the small amount of Fe^0 left after S-nZVI aging, the relatively high k_{aged} values may be partly explained by the higher pH (pH = 10.5−11.4), as argued for the CO_3^{2-} system (section 3.2.4) (Rajajayavel and Ghoshal, 2015; Wolthers et al., 2005; Kim et al., 2013) . Additionally, magnetite is electron conductive and could also facilitate electron transfer (Liu et al., 2006; Culpepper et al., 2018), but arguably at rates lower than by S-nZVI. Overall however, while the favourable pH conditions seem to uphold k_{aged} values, it is expected that continuous interaction between NO_3^- and S-nZVI would ultimately consume all Fe^0, thus compromise the reduction of target contaminants.

3.4. Influence of HPO_4^{2-}

Vivianite ($Fe_3(PO_4)_2 \cdot 8H_2O$) was the main corrosion product observed by HEXRD when S-nZVI was aged in phosphate (HPO_4^{2-}) solutions (Fig. 4d). These observations are consistent with SEM images, which show abundant rectangular sheet-like structures, typical of vivianite (Fig. 4e) (Rothe et al., 2016) . In terms of TCE reactivity, k_{aged} values were dramatically lower than in any other considered system, e.g., ~80% lower than k_{aged} of S-nZVI aged in MilliQ water (Fig. 4f, Fig. S6).

The formation of vivianite has been previously observed when ZVI was exposed to HPO_4^{2-} containing waters (Reinsch et al., 2010; Wen et al., 2014). In addition, the presence of HPO_4^{2-} has been shown to adversely affect the removal rates of nitrobenzene, TCE, and arsenic in ZVI systems (Liu et al., 2007; Yin et al., 2012; Su and Puls, 2001). When S-nZVI was aged in HPO_4^{2-} solutions, vivianite also formed and TCE reactivity was also dramatically decreased, suggesting that HPO_4^{2-} induces similar reactions on S-nZVI and ZVI surfaces. Note that HPO_4^{2-} concentrations in groundwaters are generally lower (i.e., <0.25−10 μM) (Carlyle and Hill, 2001), than tested here due to the low solubility of phosphate minerals (Markich et al., 2001; Crannell et al., 2000). Thus, our observations may only be applicable to extreme settings, such as groundwaters contaminated by fertilizer in agricultural wetlands (Lamers, 2010).

3.5. Main controls on S-nZVI reactivity after aging in single salt solutions

From the results presented above, it is clear that aging of S-nZVI in MilliQ or single salt solutions leads to Fe^0 corrosion and secondary mineral formation, which negatively affected the observed TCE reduction rate constants. The extent of Fe^0 corrosion and type of secondary mineral formation varied among different ions, which may partially explain the differences in TCE reactivity among tested ions (Fig. 5a). However, the extent of Fe^0 corrosion and the type of corrosion product was marginally affected by the tested ion concentrations, whereas TCE reactivity (k_{obs}) systematically changed with increasing ion concentrations (Fig. 5b). Specifically, we observed that increasing concentrations of NaCl, $MgCl_2$, $NaHCO_3$, and Na_2CO_3 positively affected TCE reactivity (k_{aged}), while increasing concentrations of Na_2SO_4, $CaCl_2$, and Na_2HPO_4 negatively impacted k_{aged}. This suggests that the observed systematic TCE reactivity changes were partly driven by the presence of these solutes during TCE reduction.

For ions to inhibit TCE reduction, they must lower FeS_m sites accessibility either through direct adsorption or outer-sphere complexation, or indirectly by enhancing S-nZVI aggregation. Phosphate is well known to adsorb to Fe phases (Krom and Berner, 1980), which could explain the large decrease in TCE k_{obs} seen in phosphate solutions. Calcium often enhances aggregation of negatively charged compounds such as S-nZVI (Kim et al., 2013; Dong and Lo, 2013), which may explain the decrease in TCE k_{obs} with increasing Ca^{2+} concentration.

For ions to enhance TCE reduction, they must keep the reactive FeS_m sites free of potential inhibitors, i.e., corrosion products. Fe^0 corrosion and white rust formation were significantly reduced in Cl^- solutions, thus FeS_m sites were likely more accessible, i.e., TCE reduction was enhanced. Iron carbonates, that formed in HCO_3^- and CO_3^{2-} solutions, likely aggregate less with S-nZVI due to electrostatic repulsion (compared to white rust), thus FeS_m sites were likely also more accessible in HCO_3^- and CO_3^{2-} solutions.

Overall, however, there are still many unknowns when it comes to interpreting these ion specific effects, and more experimental work is required. As shown here, multiple paramaters and processes impact TCE reactivity, making it difficult to pinpoint the controlling factor(s) in a specific scenario. As an example, different types of corrosion products will interact differently with S-nZVI surfaces, thus aggregation behaviour and FeS_m site accessibility can differ. Additionally, as S-nZVI corrodes with aging (with the extent mainly controlled by ion type), Fe^0 sites will become exposed (and likely more so if corrosion is higher), potentially enabling TCE dehalogenation pathway other than reductive β-elimination at FeS_m sites (e.g., hydrogenolysis or hydrogenation), which in turn may also affect TCE reduction rates. Another key variable to consider is pH, which can impact the surface chemistry of S-nZVI and corrosion products, and also the activity of ions in the system.

3.5.1. Real groundwater matrices

To understand if S-nZVI longevity in complex groundwaters can be estimated from the results of experiments with single salts, structural S-nZVI modifications and changes in S-nZVI reactivity

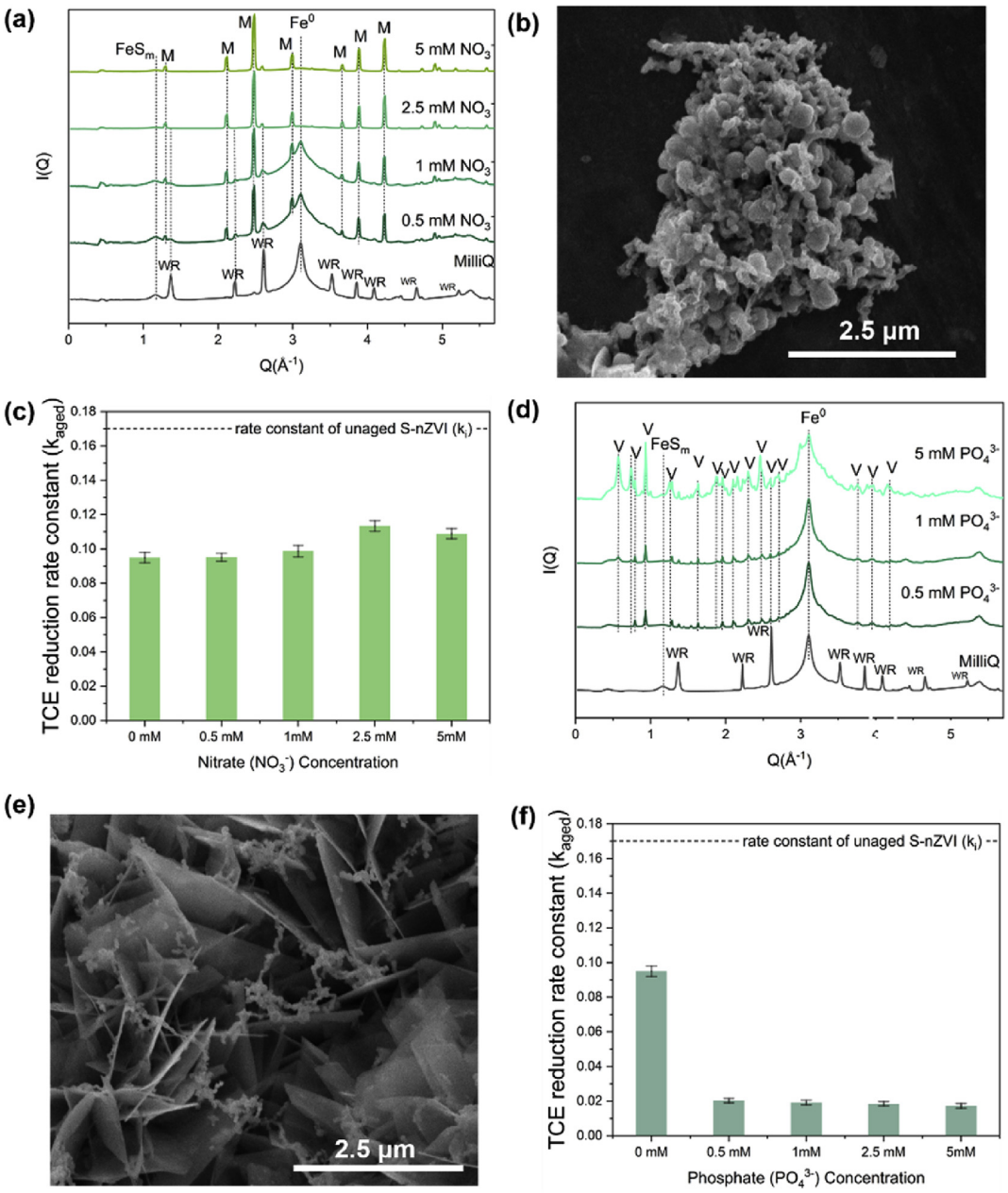

Fig. 4. a) HEXRD patterns of S-nZVI aged in varying $NaNO_3$ solutions. Magnetite (M) peaks increase in intensity while the Fe^0 core peak decreases with increasing NO_3^- concentrations. b) SEM image of S-nZVI aged in 5 mM NO_3^- showing cubic like particles, consistent with magnetite. (c) TCE reduction rate constants for S-nZVI aged in varying NO_3^- solutions. d) HEXRD patterns of S-nZVI aged in varying $NaPO_4$ solutions, with vivianite ($Fe_3(PO_4)_2 \cdot 8H_2O$, V) reflections. (e) SEM image of S-nZVI aged in a 5 mM PO_4^{3-} showing thin sheets, consistent with vivianite. f) TCE reduction rate constants for S-nZVI aged in varying PO_4^{3-} solutions.

after aging were also assessed for two types of groundwaters. S-nZVI aged in groundwater collected from the Danish site, characterized by its hardness, (i.e., GW_{HARD}; HCO_3^- = ~6.3 mM, SI, Table S1), exhibit small but noticeable HEXRD peaks that are consistent with chukanovite (SI, Fig. S8). On the other hand, S-nZVI aged in groundwater collected from the Spanish site, characterized by its high salinity (i.e., GW_{SALINE}; Cl^- = ~570 mM, SI, Table S1), exhibit characteristic peaks of chloride green rust. These observations somewhat match with the corrosion products identified in single solute systems. Chukanovite was the dominant oxidation product in high HCO_3^- solutions (5–10 mM) and in GW_{HARD}. Chloride green rust formed in high Cl^- solution (700 mM) and in GW_{SALINE}. The presence of high HCO_3^- concentrations (3.7 mM) in GW_{SALINE} may have triggered the formation of Fe^{3+} (section 3.2.4), rather than by accidential oxidation. In terms of TCE reduction rates, S-nZVI aged in GW_{HARD} and GW_{SALINE} exhibited k_{aged} of 0.09 h^{-1} and 0.12 h^{-1}, respectively (SI, Table S2, Fig. S6). These values are lower than determined for single salt solution, having comparable hardness (i.e., 5 mM HCO_3^-; 0.14 h^{-1}) or salinity (i.e., 700 mM Cl^-; 0.16 h^{-1}).

The observation that the dominant groundwater ion(s) likely control the corrosion product of S-nZVI is a valuable insight because this could help predict secondary redox reactions or sorption processes by these corrosion products. For example, it has been shown that TCE can be reduced by magnetite in the presence of aqueous Fe^{2+} (Culpepper et al., 2018), and green rust has been shown to play

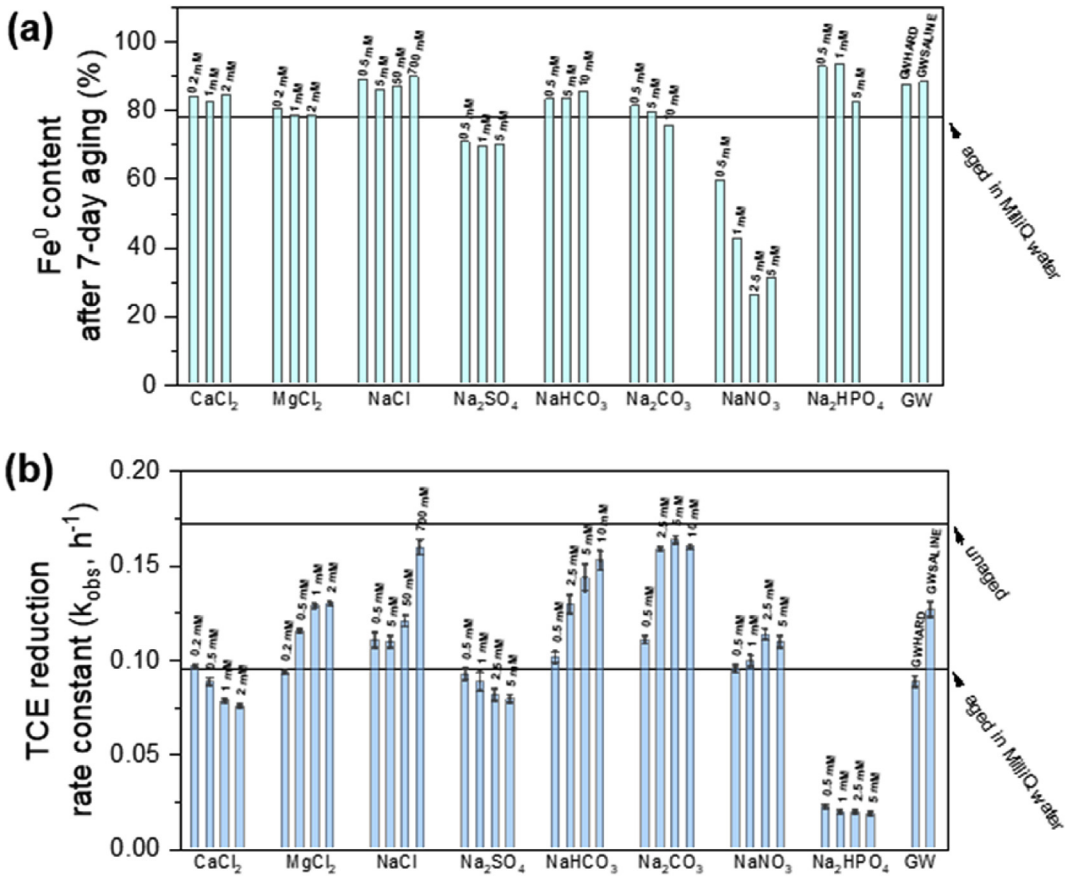

Fig. 5. a) Comparison of S-nZVI Fe^0 content after 7-day aging in different salt solutions and two types of groundwater. The solid line represents the Fe^0 content of S-nZVI aged for 7 days in MilliQ water. b) Comparison of TCE reduction rate constant (k_{obs}) by S-nZVI aged in different salt solutions and two types of groundwater. Solid lines represent k_{obs} for unaged S-nZVI and S-nZVI aged in MilliQ water for 7 days.

an active role in the redox chemistry of some common groundwater pollutants such as NO_3^- and CrO_4^{3-} (Skovbjerg et al., 2006; Alidokht et al., 2016; Hansen et al., 2001). The observation that k_{aged} in groundwater experiments were lower than expected from the single salt system may not be surprising. This mismatch may be attributed to the multitude of other, less dominant groundwater components, which may have additionally influenced TCE reactivity. For example, the presence of Ca^{2+} in GW_{HARD} (3.7 mM) and GW_{SALINE} (12.7 mM), which we showed to negatively impact TCE reduction rates even at lower concentrations (0.2–2 mM, Fig. 2c), may have influenced the observed k_{aged} values. Our groundwater analyses also show the presence of dissolved organic carbon (<2 mg L^{-1}, Table S2). Previous studies showed that even low concentrations of humic acid (HA, 5 mg L^{-1}) can lead to a 10% decrease in TCE reduction rates by S-nZVI, explained by adsorption to active FeS surface sites (Kim et al., 2013; Han et al., 2019; Bhattacharjee et al., 2016). However, they also showed that the presence of Mg^{2+} and Ca^{2+} ions can alleviate this inhibition, likely because they complex HA in solution, i.e., limit HA adsorption to S-nZVI surfaces. In another study, Suwannee River humic acid (SRH) was shown to enhance S-nZVI corrosion, leading to the formation of a non-conductive film that negatively affected TCE reactivity (Han et al., 2019). In these tests, only $NaHCO_3$ was added as a buffer, thus further tests are required to evaluate whether such corrosion enhancement and rate inhibition would also be observed in real groundwaters. Overall, while the natural organic matter was very low in the two tested groundwaters, it could still have contributed to the observed lower TCE reduction rates compared to the single salt systems. This certainly warrants further investigations that specifically evaluate the effect of competitive reactions between groundwater solutes and natural organic matter on S-nZVI longevity and reactivity. A last point to consider, pHs in the well buffered groundwaters were about a unit lower compared to single salt systems, meaning S-nZVI aged in the groundwater had a lower number of deprotonated FeS_m sites, which could also explain the lower reactivity in GW systems compared to the single salt systems (SI, Table S2).

4. Conclusion

For the first time, the impact of common groundwater ions on S-nZVI structure and reactivity during aging was investigated. Regardless of aqueous composition, 7-day aging negatively impacted TCE reduction rates because of Fe^0 corrosion and secondary mineral formation. Notably, the presence of increasing concentrations of Cl^-, Mg^{2+}, HCO_3^-, CO_3^{2-}, NO_3^- somewhat counterbalanced this reactivity loss, while the presence of SO_4^{2-}, Ca^{2+}, and PO_4^{3-} further lowered reactivity. The overall variability in TCE reactivity as a function of aqueous composition was explained by the combined effects of S-nZVI corrosion extent, type of corrosion product, pH of the system, and specific ion effects.

In the two tested groundwaters, characterized by high HCO_3^- (6.3 mM, GW_{HARD}) or high Cl^- (564 mM, GW_{SALINE}), TCE reduction rates were clearly affected by the complex ion matrices and buffered pH conditions, which led to k_{aged} values that were lower in comparison to their equivalent single salt systems (5 mM HCO_3^- and

700 mM Cl^-). These results contribute to the understanding of the fate and transport of S-nZVI in subsurface conditions; and help to predict possible secondary reactions enabled by the corrosion products. In addition, these data could serve as a benchmark to help improve the evaluation of S-nZVI fate and reactivity in various groundwater chemistries, especially aquifers polluted with TCE.

CRediT authorship contribution statement

Marco C. Mangayayam: Conceptualization, Investigation, Writing - original draft. **Virginia Alonso-de-Linaje:** Methodology, Resources. **Knud Dideriksen:** Software, Validation, Formal analysis, Funding acquisition, Supervision. **Dominique J. Tobler:** Writing - review & editing, Supervision, Funding acquisition, Project administration.

Acknowledgements

This research was funded by Metal-Aid Innovative Training Network (ITN), supported by a grant from the European Commission's Marie Skłowdowska Curie Actions program under project number 675219. The authors thank Olaf Borkiewicz, Leighanne Gallington, and Kevin A. Beyer for support with X-ray total scattering measurements at APS beamline 11 ID-B, Argonne, USA. We also thank Theis Brock-Nannestad for support with GC-MS measurements. We acknowledge Eric Querat (Consorci del Parc Agrari del Baix Llobregat), Shikhar Nilabh (Amphos 21), Markus Reischer (Niras, Denmark) and Niels Døssing Overheu (Capital Region of Denmark) for their help with groundwater collection and for providing us part of the groundwater composition data. Part of the data was acquired at Advanced Photon Source, a U.S. Department of Energy (DOE) Office of Science User Facility operated for the DOE Office of Science by Argonne National Laboratory under contract no. DE-AC02-06CH11357. Support for travel to the synchrotron facility came from the Danish Council for Independent Research (via DANSCATT).

Appendix A. Supplementary data

Supplementary data to this article can be found online at https://doi.org/10.1016/j.chemosphere.2020.126137.

References

Alidokht, L., Oustan, S., Khataee, A., Neyshabouri, M.R., Reyhanitabar, A., 2016. Enhanced removal of chromate by graphene-based sulfate and chloride green rust nanocomposites. J. Taiwan Inst. Chem. Eng. 1–9, 0.

Bhattacharjee, S., Basnet, M., Tufenkji, N., Ghoshal, S., 2016. Effects of rhamnolipid and carboxymethylcellulose coatings on reactivity of palladium-doped nanoscale zerovalent iron particles. Environ. Sci. Technol. 50 (4), 1812–1820.

Biegler, C., Houchin, M.R., 1986. Siderite (FeCO3): its dissolution and interaction with stannic oxide in aqueous suspensions. Colloid. Surface. 21 (C), 267–278.

Butler, E.C., Hayes, K.F., 1998. Effects of solution composition and PH on the reductive dechlorination of hexachloroethane by iron sulfide. Environ. Sci. Technol. 32 (9), 1276–1284.

Butler, E.C., Hayes, K.F., 2001. Factors influencing rates and products in the transformation of trichloroethylene by iron sulfide and iron metal. Environ. Sci. Technol. 35 (19), 3884–3891.

Carlyle, G.C., Hill, A.R., 2001. Groundwater phosphate dynamics in a river riparian zone: effects of hydrologic flowpaths, lithology and redox chemistry. J. Hydrol 247 (3–4), 151–168.

Chen, J.L., Al-Abed, S.R., Ryan, J.A., Li, Z., 2001. Effects of PH on dechlorination of trichloroethylene by zero-valent iron. J. Hazard Mater. 83 (3), 243–254.

Chen, R., Chen, J., Hong, M., Zhang, W., 2016. formation of chukanovite in simulated groundwater containing CO32-. Environ. Technol. 37 (21), 2786–2792.

Crannell, B., Eighmy, T., Krzanowski, J., Eusden, J.D., Shaw, E., Francis, C., 2000. Heavy metal stabilization in municipal solid waste incineration fly ash using soluble phosphate. Waste Manag. 20, 135–148.

Culpepper, J.D., Scherer, M.M., Robinson, T.C., Neumann, A., Cwiertny, D., Latta, D.E., 2018. Reduction of PCE and TCE by magnetite revisited. Environ. Sci. Process. Impacts 20 (10), 1340–1349.

Devlin, J.F., Allin, K.O., 2005. Major anion effects on the kinetics and reactivity of granular iron in glass-encased magnet batch reactor experiments. Environ. Sci. Technol. 39 (6), 1868–1874.

Dideriksen, K., Frandsen, C., Bovet, N., Wallace, A.F., Sel, O., Arbour, T., Navrotsky, A., De Yoreo, J.J., Banfield, J.F., 2015. Formation and transformation of a short range ordered iron carbonate precursor. Geochem. Cosmochim. Acta 164, 53–70.

Dong, H., Lo, I.M.C., 2013. Influence of calcium ions on the colloidal stability of surface-modified nano zero-valent iron in the absence or presence of humic acid. Water Res. 47 (7), 2489–2496.

Drissi, S.H., Refait, P., Abdelmoula, M., Génin, J.M.R., 1995. The preparation and thermodynamic properties of Fe(II)Fe(III) hydroxide-carbonate (green rust 1); pourbaix diagram of iron in carbonate-containing aqueous media. Corrosion Sci. 37 (12), 2025–2041.

Fan, D., O'Brien Johnson, G., Tratnyek, P.G., Johnson, R.L., 2016. Sulfidation of nano zerovalent iron (NZVI) for improved selectivity during in-situ chemical reduction (ISCR). Environ. Sci. Technol. 50 (17), 9558–9565.

Fan, D., Lan, Y., Tratnyek, P.G., Johnson, R.L., Filip, J., O'Carroll, D.M., Nunez Garcia, A., Agrawal, A., 2017. Sulfidation of iron-based materials: a review of processes and implications for water treatment and remediation. Environ. Sci. Technol. 51 (22), 13070–13085.

Farrell, J., Kason, M., Melitas, N., Li, T., 2000. Investigation of the long-term performance of zero-valent iron for reductive dechlorination of trichloroethylene. Environ. Sci. Technol. 34 (3), 514–521.

Farrow, C.L., Juhas, P., Liu, J.W., Bryndin, D., Božin, E.S., Bloch, J., Proffen, T., Billinge, S.J.L., 2007. PDFfit2 and PDFgui: computer programs for studying nanostructure in crystals. J. Phys. Condens. Matter 19 (33), 1–9.

Furukawa, Y., Kim, J.W., Watkins, J., Wilkin, R.T., 2002. Formation-of ferrihydrite and associated iron corrosion products in permeable reactive barriers of zero-valent iron. Environ. Sci. Technol. 36 (24), 5469–5475.

Génin, J.M.R., Aïssa, R., Géhin, A., Abdelmoula, M., Benali, O., Ernstsen, V., Ona-Nguema, G., Upadhyay, C., Ruby, C., 2005. Fougerite and FeII-IIIhydroxycarbonate green rust; ordering, deprotonation and/or cation substitution; structure of hydrotalcite-like compounds and mythic ferrosic hydroxide Fe(OH)(2+x). Solid State Sci. 7 (5), 545–572.

Gu, Y., Wang, B., He, F., Bradley, M.J., Tratnyek, P.G., 2017. Mechanochemically sulfidated microscale zero valent iron: pathways, kinetics, mechanism, and efficiency of trichloroethylene dechlorination. Environ. Sci. Technol. 51 (21), 12653–12662.

Han, Y., Ghoshal, S., Lowry, G.V., Chen, J., 2019. A comparison of the effects of natural organic matter on sulfidated and nonsulfidated nanoscale zerovalent iron colloidal stability, toxicity, and reactivity to trichloroethylene. Sci. Total Environ. 671, 254–261.

Hansen, H.C.B., Guldberg, S., Erbs, M., Bender Koch, C., 2001. Kinetics of nitrate reduction by green rusts-effects of interlayer anion and Fe(II):Fe(III) ratio. Appl. Clay Sci. 18 (1–2), 81–91.

Johnson, T.; Fish, W.; Gorby, Y.; Tratnyek, P. Degradation of carbon tetrachloride by iron metal: Complexation effects on the oxide surface http://www.sciencedirect.com/science/article/pii/S0169772297000636.

Kim, E.J., Kim, J.H., Azad, A.M., Chang, Y.S., 2011. Facile synthesis and characterization of Fe/FeS nanoparticles for environmental applications. ACS Appl. Mater. Interfaces 3 (5), 1457–1462.

Kim, E.J., Murugesan, K., Kim, J.H., Tratnyek, P.G., Chang, Y.S., 2013. Remediation of trichloroethylene by fes-coated iron nanoparticles in simulated and real groundwater: effects of water chemistry. Ind. Eng. Chem. Res. 52 (27), 9343–9350.

Kim, E.J., Kim, J.H., Chang, Y.S., Turcio-Ortega, D., Tratnyek, P.G., 2014. Effects of metal ions on the reactivity and corrosion electrochemistry of Fe/FeS nanoparticles. Environ. Sci. Technol. 48 (7), 4002–4011.

Krom, M.D., Berner, R.A., 1980. Adsorption of phosphate in anoxic marine sediments. Limnol. Oceanogr. 25 (5), 797–806.

Lamers, L.P.M., 2010. How nitrate leaching from agricultural lands provokes phosphate eutrophication in groundwater fed wetlands: the sulphur bridge. Biogeochemistry 98, 1–7.

Liu, Y., Lowry, G.V., 2006. Effect of particle age (Fe0 content) and solution PH on NZVI reactivity: H2 evolution and TCE dechlorination. Environ. Sci. Technol. 40 (19), 6085–6090.

Liu, C.C., Tseng, D.H., Wang, C.Y., 2006. Effects of ferrous ions on the reductive dechlorination of trichloroethylene by zero-valent iron. J. Hazard Mater. 136 (3), 706–713.

Liu, Y., Phenrat, T., Lowry, G.V., 2007. Effect of TCE concentration and dissolved groundwater solutes on NZVI-promoted TCE dechlorination and H2evolution. Environ. Sci. Technol. 41 (22), 7881–7887.

Liu, T., Li, X., Waite, T.D., 2013. Depassivation of aged Fe 0 by inorganic salts: implications to contaminant degradation in seawater. Environ. Sci. Technol. 47 (13), 7350–7356.

Liu, T., Li, X., Waite, T.D., 2014. Depassivation of aged Fe0 by divalent cations: correlation between contaminant degradation and surface complexation constants. Environ. Sci. Technol. 48 (24), 14564–14571.

Mangayayam, M.C., Dideriksen, K., Tobler, D.J., 2018. Can or cannot green rust reduce chlorinated ethenes? Energy Procedia 146, 173–178.

Mangayayam, M.C., Perez, J.P.H., Dideriksen, K., Freeman, H.M., Bovet, N., Benning, L.G., Tobler, D.J., 2019a. Structural transformation of sulfidized zerovalent iron and its impact on long-term reactivity. Environ. Sci. Nano submitted for publication.

Mangayayam, M., Dideriksen, K., Ceccato, M., Tobler, D.J., 2019b. The structure of

sulfidized zero-valent iron by one-pot synthesis: impact on contaminant selectivity and long-term performance. Environ. Sci. Technol. 53 (8), 4389–4396.
Markich, S.J., Brown, P.L., Jeffree, R.A., 2001. Divalent metal accumulation in freshwater bivalves: an inverse relationship with metal phosphate solubility. Sci. Total Environ. 275 (1–3), 27–41.
Morse, J.W., Arakaki, T., 1993. Adsorption and coprecipitation of divalent metals with mackinawite (FeS). Geochem. Cosmochim. Acta 57 (15), 3635–3640.
Parbs, A., Ebert, M., Dahmke, A., 2007. Long-term effects of dissolved carbonate species on the degradation of trichloroethylene by zerovalent iron. Environ. Sci. Technol. 41 (1), 291–296.
Parks, G.A., 1965. The isoelectric points of solid oxides, solid hydroxides, and aqueous hydroxo complex systems. Chem. Rev. 65 (2), 177–198.
Pekov, I., Perchiazzi, N., Merlino, S., Kalachev, V., Merlini, M., Aleksandr, Z., 2007. Chukanovite, Fe2(CO3)(OH)2, a new mineral from the weathered iron meteorite dronino. Eur. J. Mineral 19 (6), 891–898.
Po, H.N., Sutin, N., 1968. The stability constant of the monochloro complex of iron(II). Inorg. Chem. 7 (3), 621–624.
Rajajayavel, S.R.C., Ghoshal, S., 2015. Enhanced reductive dechlorination of trichloroethylene by sulfidated nanoscale zerovalent iron. Water Res. 78, 144–153.
Reardon, E.J., 1995. Anaerobic corrosion of granular iron: measurement and interpretation of hydrogen evolution rates. Environ. Sci. Technol. 29 (12), 2936–2945.
Reinsch, B.C., Forsberg, B., Penn, R.L., Kim, C.S., Lowry, G.V., 2010. Chemical transformations during aging of zerovalent iron nanoparticles in the presence of common groundwater dissolved constituents. Environ. Sci. Technol. 44 (9), 3455–3461.
Roldan, A., Hollingsworth, N., Roffey, A., Islam, H.U., Goodall, J.B.M., Catlow, C.R.A., Darr, J.A., Bras, W., Sankar, G., Holt, K.B., et al., 2015. Bio-inspired CO2conversion by iron sulfide catalysts under sustainable conditions. Chem. Commun. 51 (35), 7501–7504.
Rothe, M., Kleeberg, A., Hupfer, M., 2016. The occurrence, identification and environmental relevance of vivianite in waterlogged soils and aquatic sediments. Earth Sci. Rev. 158, 51–64.
Schott, H., 1977. Relationship between zero point of charge and solubility product for hydroxides of polyvalent cations. J. Pharmacol. Sci. 66 (11), 1548–1550.
Skovbjerg, L.L., Stipp, S.L.S., Utsunomiya, S., Ewing, R.C., 2006. The mechanisms of reduction of hexavalent chromium by green rust sodium sulphate: formation of Cr-goethite. Geochem. Cosmochim. Acta 70 (14), 3582–3592.
Su, C., Puls, R.W., 2001. Arsenate and arsenite removal by zerovalent iron: effects of phosphate, silicate, carbonate, borate, sulfate, chromate, molybdate, and nitrate, relative to chloride. Environ. Sci. Technol. 35 (22), 4562–4568.
Su, Y. fan, Hsu, C.Y., Shih, Y. hsin, 2012. Effects of various ions on the dechlorination kinetics of hexachlorobenzene by nanoscale zero-valent iron. Chemosphere 88 (11), 1346–1352.
Wen, Z., Zhang, Y., Dai, C., 2014. Colloids and surfaces A: physicochemical and engineering aspects removal of phosphate from aqueous solution using nanoscale zerovalent iron (NZVI). Colloids Surf. A Physicochem. Eng. Asp. 457, 433–440.
Wolthers, M., Charlet, L., van Der Linde, P., Rickard, D., van Der Weijden, C., 2005. Surface chemistry of disordered mackinawite (FeS). Geochem. Cosmochim. Acta 69 (14), 3469–3481.
Xu, J., Wang, Y., Weng, C., Bai, W., Jiao, Y., Kaegi, R., Lowry, G.V., 2019. Reactivity, selectivity, and long-term performance of sulfidized nanoscale zerovalent iron with different properties. Environ. Sci. Technol. 53, 5936–5945.
Yang, Y., Akid, R., 2015. Electrochemical investigation of the corrosion of different microstructural phases of X65 pipeline steel under saturated carbon dioxide conditions. Materials 8 (5), 2635–2649.
Yin, W., Wu, J., Li, P., Wang, X., Zhu, N., Wu, P., Yang, B., 2012. Experimental study of zero-valent iron induced nitrobenzene reduction in groundwater: the effects of PH, iron dosage, oxygen and common dissolved anions. Chem. Eng. J. 184, 198–204.
Yoon, R.H., Salman, T., Donnay, G., 1979. Predicting points of zero charge of oxides and hydroxides. J. Colloid Interface Sci. 70 (3), 483–493.